Volume 11
Number 1
7 January 2023
Pages 1–330

Journal of Materials Chemistry C

Materials for optical, magnetic and electronic devices

rsc.li/materials-c

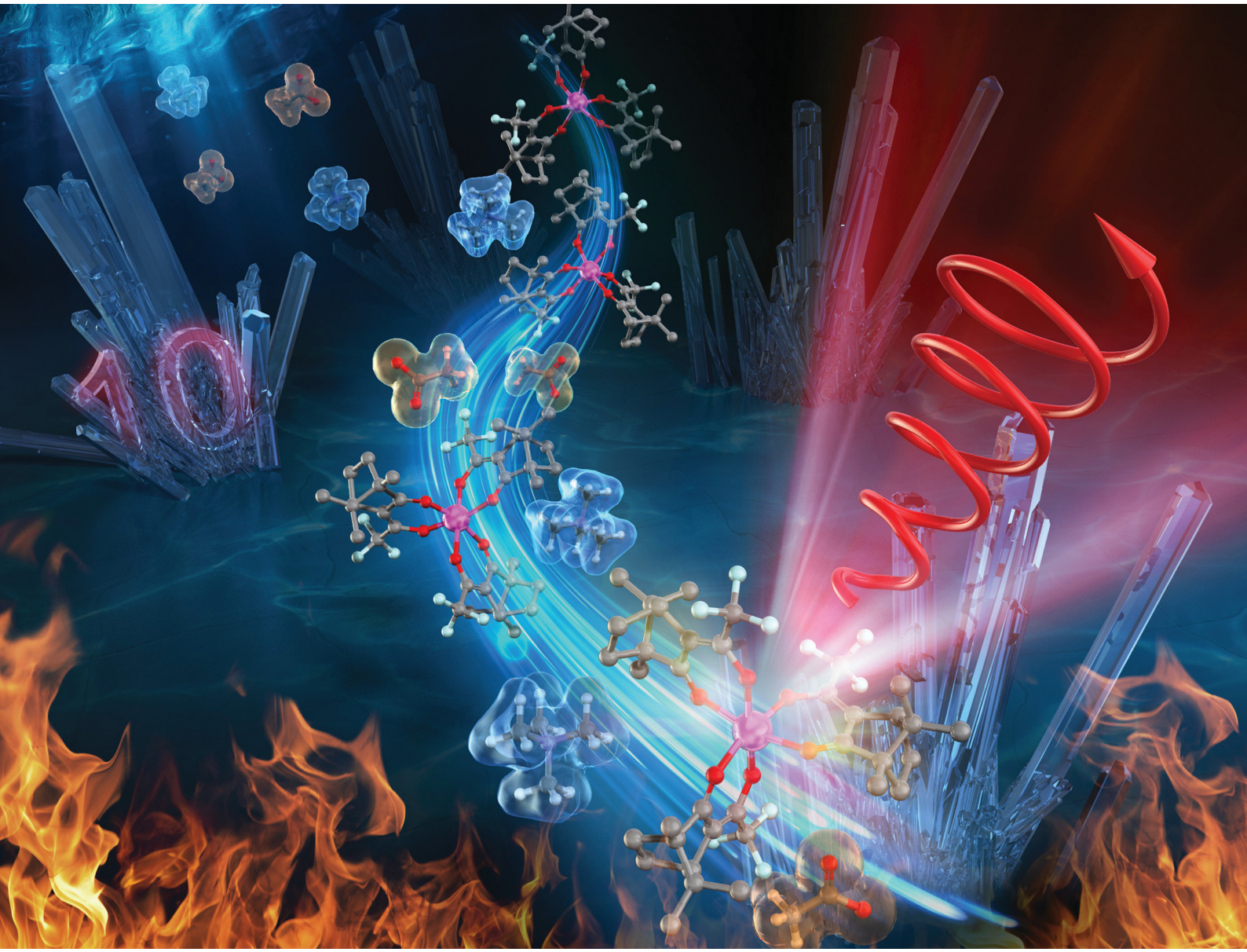

ISSN 2050-7526

ROYAL SOCIETY OF CHEMISTRY

PAPER

Norihisa Kobayashi *et al.*

Thermally stable and strongly emitted CPL in Eu(D-facam)$_3$ hybrid solids with an alkylammonium salt

10 YEARS ANNIVERSARY

Journal of Materials Chemistry C

ROYAL SOCIETY OF CHEMISTRY

PAPER

View Article Online
View Journal | View Issue

Cite this: J. Mater. Chem. C, 2023, 11, 118

Thermally stable and strongly emitted CPL in Eu(D-facam)$_3$ hybrid solids with an alkylammonium salt†

Ziying Li, Kazuki Nakamura and Norihisa Kobayashi *

Received 3rd November 2022,
Accepted 27th November 2022

DOI: 10.1039/d2tc04670a

rsc.li/materials-c

A novel europium-based hybrid material, Eu(D-facam)$_3$-TMAOAc (tetramethylammonium acetate), with ultra-high luminescence, excellent circular polarization and remarkable thermostability was prepared. Its photophysical performance was studied based on the luminescence properties and energy transfer process. Compared to Eu(D-facam)$_3$, Eu(D-facam)$_3$-TMAOAc exhibited much brighter luminescence and stronger circular polarization. Additionally, Eu(D-facam)$_3$-TMAOAc well retained its structure and luminescence properties even after heat treatment at 200 °C for 24 hours, whereas Eu(D-facam)$_3$ rapidly decomposed. Eu(D-facam)$_3$-TMAOAc was characterized by TG analysis, elemental analysis, ESI-mass spectrometry, PXRD, and FT-IR spectroscopy. It was found that TMAOAc acted as a bidentate bridge linker with Eu(D-facam)$_3$ at a 1 : 1 ratio. This coordination structure contributed to the excellent photophysical properties and thermal stability of Eu(D-facam)$_3$-TMAOAc. Furthermore, Eu(D-facam)$_3$-TMAOAc showed a high solubility in common organic solvents, and it could maintain its outstanding luminescence properties in solid as well as solution states.

Introduction

Trivalent lanthanide complexes have attracted considerable attention owing to their characteristic luminescence properties including sharp and abundant emission lines, long emission lifetime, and large pseudo-Stokes shifts for high transparency in the visible light range. They are promising materials in widespread applications such as bio-probing, bio-sensing[1–6] and electroluminescent devices.[7–10] These complexes are also expected to act as potential circularly polarized luminescence (CPL) luminophores. CPL spectroscopy measures the differential emission intensity of the right and left circularly polarized light, and thus reflects the excited state of chiral luminophores.[11] At a certain particular emission wavelength, the dissymmetry factor of CPL (g_{lum}) is defined as $2(I_L - I_R)/(I_L + I_R)$, where I_L (I_R) is the intensity of the left (right) circularly polarized luminescence. Chiral lanthanide complexes are potential candidates for CPL luminophores because they show high values of g_{lum}, two orders of magnitude greater than those observed in organic luminophores.[11] The interest in CPL has significantly increased with the development of highly sensitive bioassays[12,13] and high-resolution 3D displays.[9,14,15] Despite most of these applications preferring solid-state luminophores with high CPL activities, there are few solid-state complexes with CPL reported[16,17] (S1, ESI†). In addition, materials with both high luminescence and circular polarization are rarely reported even in the solution state. Moreover, the poor thermal stability of lanthanide complexes also significantly limits their practical applications.[18,19] The preparation of a highly luminescent material with effective CPL and outstanding thermostability is therefore of primary importance.

In recent decades, hybrid lanthanide materials such as coordination polymers,[20,21] metal–organic frameworks,[22–24] and nanocomposites,[25,26] have become a focus of considerable research interest. This is because lanthanide-based hybrid materials have a better emission output and thermal stability than single lanthanide complexes owing to their hybridized structures.[18] In these lanthanide hybrid systems, carboxylate compounds are widely used as a linkage between lanthanide ions,[5,18,21,22] because lanthanide ions are hard Lewis acids and tend to interact with hard anions such as carbonate and carboxylate ions.[27]

In our previous study, the Eu(III) complex (Eu(D-facam)$_3$) was observed to exhibit outstanding luminescence performance in the presence of tetramethylammonium acetate (TMAOAc) in alcohol.[28,29] It was found that the interaction between Eu(D-facam)$_3$ and TMAOAc contributed to a significant improvement in the luminescence properties of Eu(D-facam)$_3$ in solution. However, solid systems which toward device fabrication and

Graduate School of Engineering, Chiba University, 1-33 Yayoi-cho, Inage-ku, Chiba, 263-8522, Japan. E-mail: koban@faculty.chiba-u.jp

† Electronic supplementary information (ESI) available. See DOI: https://doi.org/10.1039/d2tc04670a

practical applications of this excellent circularly polarized luminescent Eu(III) material have not been investigated yet. In this study, a new Eu(III) hybrid material, Eu(D-facam)$_3$-TMAOAc, was successfully obtained in a solid state from Eu(D-facam)$_3$/TMAOAc mixed solutions. It was revealed that TMAOAc acts as a bidentate bridge with a function of linking Eu^{3+} ions, leading to a chain structure similar to that of coordination polymers. The photophysical properties, thermal behaviours, and coordination structures of Eu(D-facam)$_3$-TMAOAc were investigated in detail. This Eu(III) hybrid material exhibited outstanding luminescence properties, remarkable superiority in CPL activity and thermal stability in the solid state, showing its considerable potential for practical CPL applications.

Experimental section

Materials

All chemicals were commercially available and were used as received. Europium tris[3-(trifluoromethylhydroxymethylene)-(+)-camphorate] (Eu(D-facam)$_3$) and tetramethylammonium acetate (TMAOAc) were purchased from Sigma-Aldrich, Japan. The solvents, 1-butanol and acetone, were purchased from Tokyo Chemical Industry Co. Ltd, Japan.

Measurement and characterization

Oxygen dissolved in the Eu(III) compound solution was removed by bubbling nitrogen gas through the solution before carrying out optical measurements. The absorption and reflectance spectra were acquired using a UV-visible/NIR spectrophotometer (V-770, JASCO Corporation, Japan). The absorption and circular dichroism (CD) spectra of Eu(D-facam)$_3$-TMAOAc solutions were acquired using a circular dichroism spectrometer (J-1100, JASCO Corporation, Japan). The photoluminescence spectra were acquired using a spectrofluorometer (FP-6800, JASCO Corporation, Japan). The circularly polarized luminescence (CPL) measurements were conducted using a previously reported system.[30] This system consists of the following components: a 375 nm LED (M365L2, Thorlabs Japan Inc., Japan), an LED driver (DC2100, Thorlabs Japan Inc., Japan), a photoelastic modulator (PEM-90, Hinds Instruments Inc., United States), a photomultiplier tube (H7732-10, Hamamatsu Photonics K. K., Japan), a linearly polarized cubic prism (200 000 : 1), a photomultiplier tube (H7732-10, Hamamatsu Photonics K. K., Japan), and a dual-phase DSP (digital signal processing) lock-in amplifier (7265, Signal Recovery Ltd, United Kingdom). The appropriate detection wavelengths of the monochromator and the PEM (photoelastic modulator) were controlled using a PC (Dell D11M). Thermogravimetric analysis (TG) spectra were acquired using a thermogravimetry/differential thermal analyzer (TG/DTA6300, Seiko Instruments Inc., Japan). Elemental analysis was performed using a CHN/O/S elemental analyzer (CE-440F, Exeter Analytical, Inc., United States). Electrospray ionization (ESI) mass spectra were acquired using a hybrid ion trap mass spectrometer (LTQ Orbital XL, Thermo Fisher Scientific, United States). Fourier-transform infrared (FT-IR) spectra were obtained using a FT-IR spectrometer (FT/IR 680, JASCO Corporation, Japan). Powder diffraction (PXRD) spectra were acquired using a powder X-ray diffractometer (D8 ADVANCE, Bruker AXS, United States).

Preparation of Eu(D-facam)$_3$-TMAOAc

A solution of Eu(D-facam)$_3$ (89.37 mg, 0.1 mmol) in 1-butanol (10 ml, 10 mmol L^{-1}) was added to a solution of TMAOAc (66.60 mg, 0.5 mmol) in 1-butanol (10 ml, 50 mmol L^{-1}). Eu(D-facam)$_3$ is a yellow powder, and its highly concentrated (>5 mmol L^{-1}) 1-butanol solution shows a pale-yellow colour. By addition of TMAOAc solution, the yellow colour of Eu(D-facam)$_3$ solution quickly disappeared and the solution became transparent. A white precipitate was observed in the transparent mixed solution only within 1 h after mixing. The mixture solution without stirring was set aside for 48 h, and the white precipitate was filtered, thoroughly washed with deionized water, and allowed to dry *in vacuo*.

Results and discussion

Luminescence performance of Eu(D-facam)$_3$-TMAOAc

The absorption spectra of Eu(D-facam)$_3$ and the Eu(D-facam)$_3$/TMAOAc mixed solution were recorded, and they are shown in Fig. 1. The concentration of Eu(D-facam)$_3$ was fixed at 0.5 mmol L^{-1} for fair comparison. The absorbance peaks at approximately 300 nm were ascribed to π–π* transition of ligands and were not affected by adding TMAOAc. At high concentration (10 mmol L^{-1}) of Eu(III) compounds, colour change of solution was directly observed on addition of TMAOAc. As shown in the Fig. 1 inset, a tiny peak in both solutions at 465 nm was derived from $^5D_2 \leftarrow {}^7F_0$ transition.[31] In the spectra of Eu(D-facam)$_3$ solution, a broad band appeared around 400 nm∼ owing to the observed yellow colour. On the other hand, in the spectra of the Eu(D-facam)$_3$/TMAOAc mixed solution, a lower absorption band was observed at the same wavelength, indicating that the solution was colourless and

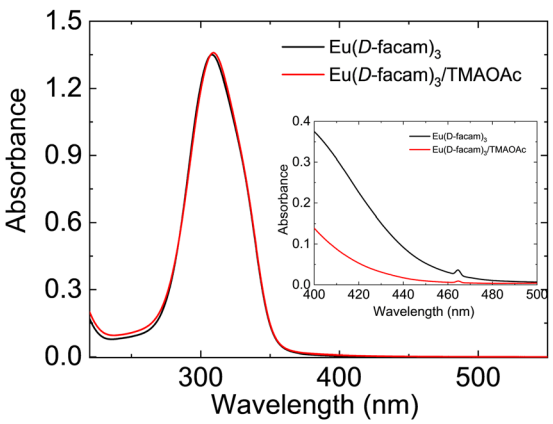

Fig. 1 Absorption spectra of Eu(D-facam)$_3$ and the Eu(D-facam)$_3$/TMAOAc mixed solution in 1-butanol. The concentration was fixed to 0.5 mmol L^{-1} and 10 mmol L^{-1} (inset).

transparent. The colour bleaching that occurred in the solution suggested a rapid interaction between Eu(D-facam)$_3$ and TMAOAc in 1-butanol. The alteration of colour in both solution and solid systems confirmed the successful fabrication of the new Eu(III) hybrid material, Eu(D-facam)$_3$-TMAOAc.

Fig. 2(a) shows digital photographs of Eu(D-facam)$_3$ and Eu(D-facam)$_3$-TMAOAc upon irradiation with a UV lamp (λ = 365 nm). Clearly, Eu(D-facam)$_3$-TMAOAc exhibited a much stronger red luminescence than that of Eu(D-facam)$_3$. In order to characterize the luminescence properties of Eu(D-facam)$_3$-TMAOAc, normalized emission spectra of Eu(D-facam)$_3$ and Eu(D-facam)$_3$-TMAOAc in the solid state were obtained (Fig. 2(b)). The original emission spectra (inset in Fig. 2(b)) of Eu(D-facam)$_3$-TMAOAc exhibited a dramatic increase compared to Eu(D-facam)$_3$ spectra, which is in agreement with the visually observed luminescence shown in Fig. 2(a). The characteristic bands of the Eu(III) complex corresponding to the $^5D_0 \rightarrow {}^7F_J$ (J = 0–3) transitions are observed at approximately 575, 595, 612 and 650 nm. $^5D_0 \rightarrow {}^7F_0$ transition was reported as an indicator for Eu(III) complexes in specific symmetry systems.[32–34] The emission peak derived from $^5D_0 \rightarrow {}^7F_0$ transition in Eu(D-facam)$_3$ cannot be observed when Eu(D-facam)$_3$ is coordinated with TMAOAc, indicating that Eu(D-facam)$_3$-TMAOAc has a different symmetry structure from Eu(D-facam)$_3$. $^5D_0 \rightarrow {}^7F_1$ is a magnetic dipole (MD) transition, and its radiative rate is independent of the environment around Eu^{3+} ions, and the shape of the emission band directly reflects the crystal-field splitting of the $^7F_1$ level.[31] An obvious split of the emission peak related to the $^5D_0 \rightarrow {}^7F_1$ transitions in Eu(D-facam)$_3$-TMAOAc was observed, suggesting that TMAOAc perturbed the crystal fields of Eu(III) complexes. In addition, $^5D_0 \rightarrow {}^7F_2$ transitions are known to be typical electric dipole (ED) transitions that are highly sensitive to the environment around Eu^{3+} ion and the nature of ligands. The dominant emission peaks derived from $^5D_0 \rightarrow {}^7F_2$ transitions became narrower and sharper in Eu(D-facam)$_3$-TMAOAc than in Eu(D-facam)$_3$, accounting for the changed coordination structure of Eu(III) complexes caused by interactions with TMAOAc. According to the Judd–Ofelt theory, the hypersensitive $^5D_0 \rightarrow {}^7F_2$ transition is strictly forbidden for Eu^{3+} ions with a centre of symmetry, and, thus, a low-site symmetry around Eu^{3+} ions typically exhibits a more intense emission peak derived from $^5D_0 \rightarrow {}^7F_2$ transition.[31] Moreover, the emission intensity from the $^5D_0 \rightarrow {}^7F_1$ transition remains constant in the total integrated intensity and normally it is used as an 'internal reference'.[35,36] The site symmetry can thus be evaluated from the intensity ratio (I_{rel}) of the integrated intensities from $^5D_0 \rightarrow {}^7F_2$ to $^5D_0 \rightarrow {}^7F_1$ transition.[31] The values of I_{rel} for Eu(D-facam)$_3$ and Eu(D-facam)$_3$-TMAOAc were calculated to be 10.58 and 6.88, respectively, implying that the interaction between the Eu(III) complex and TMAOAc contributed to a higher site symmetry around Eu^{3+} ions in this new Eu(III) hybrid material. These changes in emission spectra could be attributed to the rearrangement of the coordination geometry in Eu(III) complexes.

The circularly polarized luminescence (CPL) of Eu(III) complexes is largely influenced by their coordination geometries. CPL measurements of Eu(D-facam)$_3$ and Eu(D-facam)$_3$-TMAOAc were performed in a solid state (in KBr pellets). The dissymmetry factor, g_{lum}, was used to quantitatively evaluate the CPL activity of both Eu(III) compounds as shown in Fig. 3. The value of g_{lum} was calculated from $2(I_L - I_R)/(I_L + I_R)$, where I_L (I_R) is the intensity of the left (right) circularly polarized luminescence. Therefore, g_{lum} can be used to evaluate the emission ratio of left or right CPL. Characteristic CPL signals were observed at approximately 585–605 and 610–620 nm, corresponding to the emissions from $^5D_0 \rightarrow {}^7F_1$ and $^5D_0 \rightarrow {}^7F_2$ transition, respectively. For $^5D_0 \rightarrow {}^7F_1$ MD transition, a high

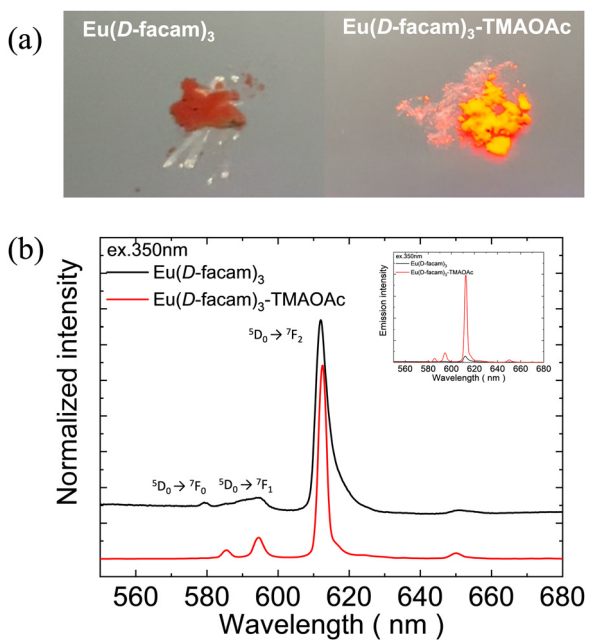

Fig. 2 (a) Digital photographs of luminescent Eu(D-facam)$_3$ (left) and Eu(D-facam)$_3$-TMAOAc(right) upon irradiation with UV light (λ = 365 nm). (b)Normalized and original(inset) emission spectra of Eu(D-facam)$_3$ and Eu(D-facam)$_3$-TMAOAc in the solid state. The excitation wavelength was 350 nm.

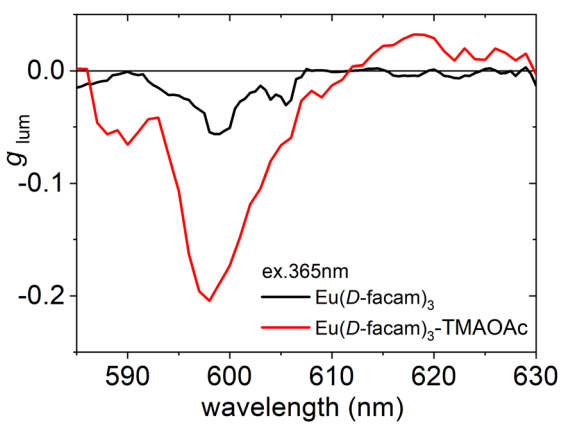

Fig. 3 g_{lum} spectra of Eu(D-facam)$_3$ and Eu(D-facam)$_3$-TMAOAc in KBr pellets. The excitation wavelength was 365 nm.

g_{lum} of −0.21 from Eu(D-facam)$_3$-TMAOAc was observed, which was more than four times higher than that of Eu(D-facam)$_3$ (g_{lum} = −0.05). The CPL properties of Eu(D-facam)$_3$ in KBr pellets, as observed in this study, agreed well with those in previous reports.[17] For the $^5D_0 \rightarrow {}^7F_2$ electronic transition, a CPL signal of Eu(D-facam)$_3$-TMAOAc (g_{lum} = +0.03) was observed, whereas no CPL was observed in Eu(D-facam)$_3$ (g_{lum} = 0). In this novel Eu(III) hybrid material, the right CPL from the $^5D_0 \rightarrow {}^7F_1$ transition was obviously enhanced (g_{lum} = −0.05 → −0.21) and left CPL from the $^5D_0 \rightarrow {}^7F_2$ transition was induced (g_{lum} = 0 → −0.03). The excellent CPL activity indicated that the chiral environment and coordination structure of Eu(D-facam)$_3$ were obviously affected because of the interaction with TMAOAc.

Furthermore, the differential absorption intensity of the light and left circularly polarized light was measured by circular dichroism (CD) spectroscopy. CD is typically used to investigate the chiral structure of materials as a complementary tool to CPL. The absorption and CD spectra of Eu(D-facam)$_3$ and Eu(D-facam)$_3$-TMAOAc were then studied in KBr pelleta (Fig. S2, ESI†). Reproducibility of the CD signal from the film samples was validated by rotating the samples to avoid the artefacts. For both Eu(III) complexes, a broad absorption band covering 300–350 nm, attributed to π–π* transition from β-diketonate ligands, was observed. In the CD measurement, Eu(D-facam)$_3$ did not exhibit any significant peaks and the lack of CD is probably responsible for a weak CPL signal.[37] An obvious positive CD peak at approximately 350 nm was observed for Eu(D-facam)$_3$-TMAOAc, indicating the changed spatial disposition of multi-chromophores of β-diketonate ligands. This change was probably ascribed to the interaction with TMAOAc, which presumably could distort the geometric structure of ligands in this Eu(III) hybrid material. The finding in chiroptical properties (CD and CPL) revealed that the interaction between Eu(D-facam)$_3$ and TMAOAc showed profound effects on the chirality of β-diketonate ligands and coordination geometry of Eu(III) complexes. These structural changes could have probably led to the altered electronic structure of Eu(III) complexes owing to TMAOAc hybridization, which can also be observed from the affected diffuse reflectance spectra of Eu(III) complexes.

In accordance with absorption spectra, diffuse reflectance spectra of both Eu(D-facam)$_3$ and Eu(D-facam)$_3$-TMAOAc in the solid state also exhibited broad peaks at approximately 350 nm from β-diketonate ligands (Fig. S3, ESI†). The variation in the shape of both Eu(III) compounds was observed, suggesting that TMAOAc affected the electrical transition of ligands in this new Eu(III) hybrid material.

Eu(D-facam)$_3$-TMAOAc presented much better luminescence performance than Eu(D-facam)$_3$ even under the condition of higher symmetry. Higher symmetry around Eu^{3+} contributed to a low radiative rate constant, leading to a low emission intensity.[38] To further elucidate the photophysical properties of Eu(III) complexes, their energy transfer process was precisely analysed. Firstly, the time-resolved emission profiles (Fig. 4) and the quantum yield of Eu(D-facam)$_3$ and Eu(D-facam)$_3$-TMAOAc in the solid state were measured (Table 1). The values

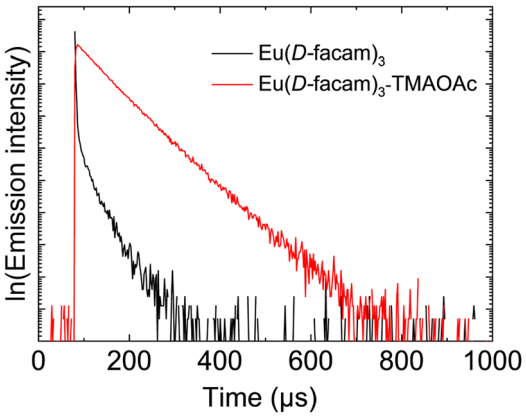

Fig. 4 Emission decay profiles of Eu(D-facam)$_3$ and Eu(D-facam)$_3$-TMAOAc in the solid state. The excitation wavelength was 350 nm.

Table 1 Luminescence lifetimes (τ), intrinsic quantum yields (Φ_{Ln}), total quantum yields (Φ_{tot}), efficiencies of sensitization (η_{sens}), radiative rates (k_r), non-radiative rates (k_{nr}), and emission intensity ratios of total to the ED moments (I_{tot}/I_{MD}) for Eu(D-facam)$_3$ and Eu(D-facam)$_3$-TMAOAc in the solid state

	I_{tot}/I_{MD}	τ (μs)	Φ_{tot} (%)	Φ_{Ln} (%)	k_r (s^{-1})	k_{nr} (s^{-1})	η_{sens} (%)
Eu(D-facam)$_3$	11.9	278.5	1.6	16.4	588.4	3002.3	9.7
Eu(D-facam)$_3$-TMAOAc	7.7	692.1	21.5	26.3	380.7	1064.2	81.6

of lifetime (τ) and quantum yield (Φ_{tot}) for Eu(D-facam)$_3$ were 278.5 μs and 1.6%, respectively. A significant enhancement was obtained in Eu(D-facam)$_3$-TMAOAc with values 692.1 μs and 21.5% for τ and Φ_{tot}, respectively, which was consistent with the photographs of the bright luminescence from Eu(D-facam)$_3$-TMAOAc as seen in Fig. 1(a).

A series of key photophysical parameters were estimated and the values are shown in Table 1. The radiative rate constant (k_r) and non-radiative rate constant (k_{nr}) were calculated as follows:

$$k_r = A_{MD} \times n^3 \times \left(\frac{I_{tot}}{I_{MD}}\right)$$

$$\tau = \frac{1}{k_r + k_{nr}}, \quad k_{nr} = \frac{1}{\tau} - k_r$$

where $A_{MD,0}$ is the spontaneous emission probability for the $^5D_0 \rightarrow {}^7F_1$ magnetic dipole transition *in vacuo* (14.65 s^{-1}), n is the refractive index of the medium (1.5 for solid) and I_{tot}/I_{MD} is the ratio of the total integrated area of the emission spectrum to the area of the $^5D_0 \rightarrow {}^7F_1$ band.

The intrinsic quantum yield (Φ_{Ln}) and sensitization efficiency of the lanthanide luminescence by the ligands (η_{sens}) was then evaluated as follows:

$$\Phi_{Ln} = \frac{k_r}{k_r + k_{nr}}, \eta_{sens} = \frac{\Phi_{tot}}{\Phi_{Ln}}$$

Compared to Eu(D-facam)$_3$, a decrease in the radiative rate constant for Eu(D-facam)$_3$-TMAOAc was observed, corresponding to its higher symmetry. This is because, in the Eu(III) complex with higher symmetry, the forbidden electric dipole transitions in the Judd–Ofelt theory would be more strictly forbidden and thus leading to a lower radiative rate constant.[31] In addition, the non-radiative rate constant for Eu(D-facam)$_3$-TMAOAc was significantly suppressed (3002.3 s^{-1} → 1064.2 s^{-1}). Under this condition, the competition ability of the radiative process for Eu(D-facam)$_3$-TMAOAc is stronger than Eu(D-facam)$_3$ in emission pathways, so a higher intrinsic quantum yield in Eu(D-facam)$_3$-TMAOAc was obtained. Therefore, superior photophysical properties were observed in Eu(D-facam)$_3$-TMAOAc even with a higher symmetry. Based on these variations, the sensitization efficiency of Eu(D-facam)$_3$-TMAOAc was significantly improved to 81.6%, obviously higher than that of Eu(D-facam)$_3$ (9.7%). Compared to an improved sensitization efficiency of 28% in the Eu(D-facam)$_3$/TMAOAc mixed solution previously reported,[28] the new Eu(III) hybrid material in this study showed a significant progress in the sensitization performance of the original Eu(D-facam)$_3$. This was likely because the interaction between Eu(III) complexes and TMAOAc decreases the distance between the Eu^{3+} ion and the β-diketonate ligands, and the shorter donor–acceptor distance can accelerate the energy transfer rate for a higher sensitization efficiency.[39]

Thermostability and interaction ratio of Eu(D-facam)$_3$-TMAOAc

It is typically difficult for lanthanide complexes to maintain a stable structure and luminescence at a high temperature for a long time, although many applications require thermal stability. Therefore, the thermal stability for the luminescence and structure of both Eu(III) compounds was investigated after a long-time heat treatment and cooling to room temperature. Emission spectra (Fig. S4, ESI†) and emission decay profiles of Eu(D-facam)$_3$ and Eu(D-facam)$_3$-TMAOAc were obtained at room temperature before and after the heat treatment at 150 °C for 24 h. The emission peaks of both Eu(III) compounds were not changed, suggesting their stable coordination structures after 150 °C heat treatment. In addition, the decrease in the emission lifetime was 9.8% for Eu(D-facam)$_3$ and 0.8% for Eu(D-facam)$_3$-TMAOAc. Therefore, both Eu(III) compounds maintained their luminescence performance after the 150 °C heat-treatment. On the other hand, a notable difference in the physical state and luminescence performance between Eu(D-facam)$_3$ and Eu(D-facam)$_3$-TMAOAc was observed upon heat treatment at 200 °C for 24 h. Eu(D-facam)$_3$ quickly melted and turned into a dark adhesive through heating at 200 °C. This could be explained by the fact that Eu(D-facam)$_3$ lost its complex structure and luminescence, which was invisible to the naked eye, upon UV irradiation (Fig. S5(a), ESI†). In contrast, Eu(D-facam)$_3$-TMAOAc well maintained its solid state and bright luminescence even after 24 h of the heat treatment at 200 °C (Fig. S5(b), ESI†). As seen in Table 2, the emission lifetime of melted Eu(D-facam)$_3$ and well maintained solid-state Eu(D-facam)$_3$-TMAOAc was 42.3 μs and 682.9 μs, respectively.

Table 2 Luminescence lifetimes for Eu(D-facam)$_3$ and Eu(D-facam)$_3$-TMAOAc before and after 24 hours of heat-treatment at 150 °C and 200 °C in the solid state

		τ (μs) after heat-treatment for 24 hours	
	τ (μs) before heat-treatment	150 °C	200 °C
Eu(D-facam)$_3$	278.5	251.2	42.3
Eu(D-facam)$_3$-TMAOAc	692.1	686.6	682.9

Eu(D-facam)$_3$-TMAOAc retained its high luminescence properties with a slight loss of 1.3% in the emission lifetime, whereas the emission lifetime of Eu(D-facam)$_3$ was reduced by 84.8%. Fourier-transform infrared spectra (FT-IR) of Eu(D-facam)$_3$-TMAOAc before and after 24 h of heat treatment at 200 °C were obtained (Fig. S6, ESI†). There was no change in FT-IR spectra before and after heat treatment, confirming the high thermal stability of the structure and physical state of Eu(D-facam)$_3$-TMAOAc, consistent with the above results. Actually, TMAOAc itself is very unstable at high temperatures above 150 °C. The improved thermal stability for both Eu(D-facam)$_3$ and TMAOAc in this new hybrid material could be ascribed to their stable interactions.

Furthermore, the red luminescence of Eu(D-facam)$_3$-TMAOAc was maintained even at high temperatures. As shown in Fig. 5(a), sharp and intense emission peaks of Eu(D-facam)$_3$-TMAOAc were observed even at 100 °C. The shape of emission peaks was consistent with that obtained from room-temperature measurements, suggesting the stable luminescence properties and coordination structure of Eu(D-facam)$_3$-TMAOAc at 100 °C. On the contrary, the luminescence of Eu(D-facam)$_3$ was totally quenched with no emission peaks at 100 °C (Fig. 5(b)). During the energy transfer process of Eu(III) complexes, the radiative rate constant (k_r) is independent of temperature, and the non-radiative rate constant (k_{nr}) is known as a temperature-dependent parameter.[40] The intrinsic quantum yield (Φ_{Ln}) can be calculated as $k_r/(k_r + k_{nr})$. In the case of Eu(D-facam)$_3$, the enhanced k_{nr} at 100 °C gave rise to a significant increase in the denominator, making Φ_{Ln} extremely close to zero. The luminescence of Eu(D-facam)$_3$ at 100 °C was thus quenched. Conversely, Eu(D-facam)$_3$-TMAOAc exhibited a much lower k_{nr} (1064.2 s^{-1} at room temperature) than Eu(D-facam)$_3$ (3002.3 s^{-1} at room temperature), so the denominator, ($k_r + k_{nr}$), at 100 °C for Eu(D-facam)$_3$-TMAOAc was much

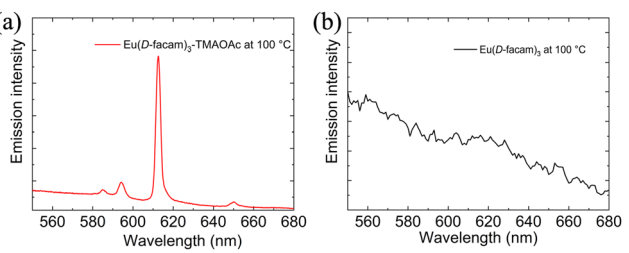

Fig. 5 Emission spectra of (a) Eu(D-facam)$_3$-TMAOAc and (b) Eu(D-facam)$_3$ at 100 °C in the solid state.

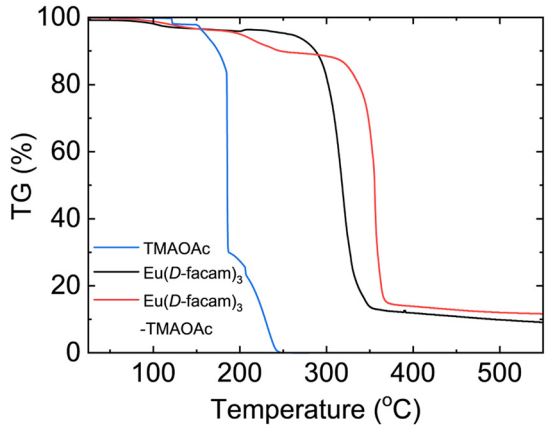

Fig. 6 TG analysis of Eu(D-facam)$_3$, TMAOAc and Eu(D-facam)$_3$-TMAOAc.

smaller than that for Eu(D-facam)$_3$. Therefore, Φ_{Ln} of Eu(D-facam)$_3$-TMAOAc at 100 °C maintained a relatively substantial value, accounting for the red luminescence even at a high temperature.

The thermal properties of Eu(D-facam)$_3$-TMAOAc were investigated by thermogravimetric (TG) analysis. Fig. 6 shows the weight-loss process of Eu(D-facam)$_3$, TMAOAc, and Eu(D-facam)$_3$-TMAOAc at 20–500 °C. Eu(D-facam)$_3$-TMAOAc showed improved thermal stability up to 320 °C, whereas a successive mass loss of Eu(D-facam)$_3$ started at 270 °C. In the case of TMAOAc, two decomposition steps were observed for TMA^+ and OAc^-, respectively. A complete thermal decomposition of TMAOAc occurred at 250 °C, accompanied by a mass loss of 100%. Interestingly, Eu(D-facam)$_3$-TMAOAc could still exhibit a brilliant luminescence after 24 h of heat treatment at 250 °C. The excellent thermal stability was ascribed to the stable structure owing to the interaction between Eu(D-facam)$_3$ and TMAOAc.

To investigate the interaction ratio of Eu(D-facam)$_3$ to TMAOAc in this new hybrid Eu(III) material, elemental analysis (for C, H, and N) was conducted. The calculated and experimental elemental compositions are shown in Table 3. The calculated values based on the interaction ratio of 1 : 1 matched well with the experimental values, and thereby the interaction ratio of Eu(D-facam)$_3$ to TMAOAc was estimated to be 1 : 1.

Moreover, Eu(D-facam)$_3$-TMAOAc, precipitated from 1-butanol with high concentrations of both starting materials, is soluble in 1-butanol at a relatively low concentration (0.2 mmol L^{-1}). Based on our previous report, a higher concentration of TMAOAc could lead to an increase in the site symmetry around Eu^{3+} ions (decreased I_{rel}) and a change in the emission peaks.[28] The emission spectra of Eu(D-facam)$_3$-TMAOAc and a mixed solution of Eu(D-facam)$_3$ and TMAOAc

Table 3 Elemental analysis of Eu(D-facam)$_3$-TMAOAc

C (%)		H (%)		N (%)	
Calcd	Found	Calcd	Found	Calcd	Found
49.13	49.50	5.60	5.59	1.36	1.33

Table 4 Results of TG-DTA analysis of Eu(D-facam)$_3$-TMAOAc

Temperature range (°C)	Mass loss (%) found (calcd)	Probable lost molecules	Residue mass (%) found (calcd)	Composition of the residue
100–320	12.90 (12.89)	TMAOAc		
320–370	72.48 (72.35)	D-facam	14.62(14.76)	Eu_2O_3

with a concentration ratio of 1 : 1 in 1-butanol were measured (Fig. S7, ESI†). The perfectly matched emission spectra and the same site symmetry (I_{rel} = 6.45) indicated that their identical coordination structures still maintained even in the solution state, further supporting the 1 : 1 interaction ratio between TMAOAc and Eu(D-facam)$_3$ in Eu(D-facam)$_3$-TMAOAc.

Based on the confirmed interaction ratio, the experimental and corresponding theoretical thermoanalytical data of Eu(D-facam)$_3$-TMAOAc are shown in Table 4. The first mass loss stage in Eu(D-facam)$_3$-TMAOAc was observed from 100 to 320 °C, which was a gradual mass loss, likely, from TMAOAc. The total loss during the first stage was 12.90%, which was close to the calculated loss percentage (12.89%), further verifying the 1 : 1 interaction ratio between Eu(D-facam)$_3$ and TMAOAc. The second main successive mass loss stage was from 320 to 370 °C, and the corresponding mass loss of 72.48% was attributed to the loss of (D-facam) ligands. The final residue was predicted to be Eu_2O_3, which was also consistent with the theoretical result. In addition, one thermal decomposition step of the ligand loss in Eu(D-facam)$_3$ occurred at 270 °C. Therefore, Eu(D-facam)$_3$-TMAOAc exhibited better thermal stability than Eu(D-facam)$_3$. The interaction between Eu(D-facam)$_3$ and TMAOAc at a 1 : 1 ratio significantly contributed to both the outstanding luminescence performance and thermal stability in Eu(D-facam)$_3$-TMAOAc.

Structure analysis of Eu(D-facam)$_3$-TMAOAc

To elucidate the impressive improvement in optical behaviours and thermal stability of this Eu(III) hybrid material, the structures and configurations were studied. Electrospray ionization (ESI) mass spectrometry of Eu(D-facam)$_3$-TMAOAc was first conducted. A series of experimental and corresponding calculated mass signals identifying the coordination structure of this Eu(III) hybrid material were obtained. All the experimental mass spectra were highly consistent with the calculated signals, ensuring the reliability of the following fragments. The fragments $[Eu(D\text{-facam})_3{\cdot}TMA]^+$, $[Eu(D\text{-facam})_3{\cdot}OAc]^-$, $[Eu(D\text{-facam})_3{\cdot}TMA{\cdot}2OAc]^-$, and $[Eu(D\text{-facam})_3{\cdot}2TMA{\cdot}OAc]^+$ (Fig. S8, ESI†) indicated the interaction between single Eu(D-facam)$_3$ and TMAOAc. $[2Eu(D\text{-facam})_3{\cdot}TMA]^+$, $[2Eu(D\text{-facam})_3{\cdot}OAc]^-$, $[2Eu(D\text{-facam})_3{\cdot}TMA{\cdot}2OAc]^-$, and $[2Eu(D\text{-facam})_3{\cdot}2TMA{\cdot}OAc]^+$ (Fig. S9, ESI†) demonstrated that multi-Eu(III) complexes were associated via TMAOAc.

It was reported that acetates could act as a bidentate ligand binding to lanthanide ions.[41] In our study, acetates probably play a similar role as a bidentate bridge to link multiple Eu^{3+} ions and form a chain structure of Eu(III) complexes. As many studies have reported, carboxylate compounds generally act as

a linkage to form a lanthanide polymer with remarkable luminescence and stability.[5,18,21,22] In such a chain structure, the distance between a donor and an accepter (ligand-Eu^{3+}) in the Eu(III) hybrid materials is typically shorter than that in a single complex. Therefore, Eu(D-facam)$_3$-TMAOAc was endowed with a significantly accelerated transfer energy (high sensitization efficiency) and enhanced emission intensity. Moreover, the Eu(III) coordination polymers are known to decrease vibrational quenching because of their chain-structural rigidness.[42] Thus, the non-radiative rate was significantly suppressed (3002.3 s^{-1} → 1064.21 s^{-1}) in Eu(D-facam)$_3$-TMAOAc with its rigid chain structures.

In our previous study concerning the solution state, the effect of a series of ammonium salts with various cations and anions on Eu(III) complexes was investigated. The results demonstrated the irreplaceability of both TMA^+ and OAc^- in the photoluminescence improvement of Eu(D-facam)$_3$. In this study, the fragments were also indicative of the importance of both TMA^+ and OAc^- in this novel Eu(III) hybrid material. TMAOAc was indispensable for the improvement of luminescence properties of Eu(D-facam)$_3$ in both solution and solid states.

Fig. 7 shows the FT-IR spectra of Eu(D-facam)$_3$, TMAOAc, and Eu(D-facam)$_3$-TMAOAc. For Eu(D-facam)$_3$, two peaks shown in the range 1500–1600 cm^{-1} suggested the C=C=C stretching vibration of the β-diketonate moiety in Eu(D-facam)$_3$.[43] The double peaks merged into one peak at around 1550 cm^{-1} in Eu(D-facam)$_3$-TMAOAc, indicating a more equivalent C=C=C bonding. In TMAOAc, the peaks at around 1560 and 1390 cm^{-1} were attributed to the antisymmetric and symmetric stretching vibration of COO^-, respectively.[44] With respect to Eu(D-facam)$_3$-TMAOAc, the COO^- antisymmetric stretching vibration shifted from 1560 to 1550 cm^{-1}, and signals at around 1420 cm^{-1} were slightly enhanced due to the COO^- symmetric stretching vibration. Nakamoto reported that the difference (delta value) between the COO^- antisymmetric and symmetric stretching frequencies could be used to determine the bonding mode of acetate groups.[45] The ionic mode (TMAOAc itself) and bridging mode (Eu(D-facam)$_3$-TMAOAc) both showed a delta value of 140–170 cm^{-1}, whereas the unidentate mode had a much larger delta value of 200–300 cm^{-1}. In Eu(D-facam)$_3$-TMAOAc, a delta value of 160 cm^{-1} was clear evidence for the bidentate-bridging role of OAc^- and its chain structure.

The hybrid material was crystallized to yield only tiny needle-like crystals. The powder X-ray diffraction (PXRD) of Eu(D-facam)$_3$-TMAOAc was conducted for structure investigation (Fig. 8). Eu(D-facam)$_3$ showed broad and weak signals which were attributed to its low crystallinity. In contrast, sharp and strong signals from Eu(D-facam)$_3$-TMAOAc were observed. Although no single crystal for the structure determination was acquired, it verified the high crystallinity of Eu(D-facam)$_3$-TMAOAc. From both ESI-mass spectrometry and PXRD measurements, Eu(D-facam)$_3$-TMAOAc presumably acted as a chain structure, and the TMAOAc linkage resulted in a change in the coordination geometry of Eu(D-facam)$_3$, as reflected from the PXRD signal shift. The preparation of a single crystal of Eu(D-facam)$_3$-TMAOAc is still going on under various crystallization conditions, and the detailed crystalline structure of this new Eu(III) hybrid material will be presented in the near future.

Solubility of Eu(D-facam)$_3$-TMAOAc

Most Eu(III)-based coordination polymer materials typically have a low solubility in organic solvents.[46] However, Eu(D-facam)$_3$-TMAOAc presented a decent solubility in most organic solvents, such as acetone, acetonitrile, chloroform, dimethyl sulfoxide and some alcohols.

Interestingly, although acetone, one of the most common organic solvents, does not dissolve TMAOAc itself, the new Eu(III) hybrid material proposed in this study can be easily dissolved in acetone. This suggested that there was a stable interaction between TMAOAc and Eu(D-facam)$_3$ in Eu(D-facam)$_3$-TMAOAc. Therefore, acetone is the optimal solvent for the investigation of the luminescence performance of Eu(D-facam)$_3$-TMAOAc in the solution state. Fig. 9 shows the emission spectra of Eu(D-facam)$_3$ and Eu(D-facam)$_3$-TMAOAc in acetone. Eu(D-facam)$_3$-TMAOAc exhibited a stronger emission

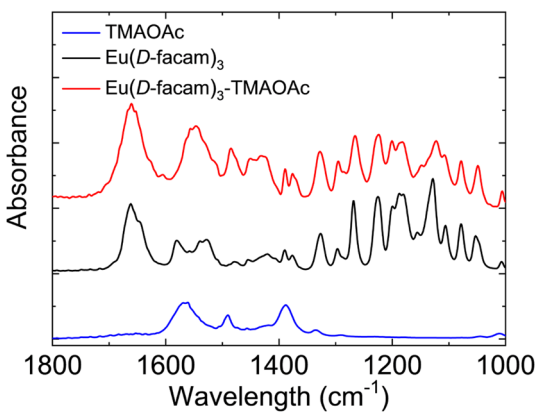

Fig. 7 FT-IR spectra of Eu(D-facam)$_3$, TMAOAc and Eu(D-facam)$_3$-TMAOAc.

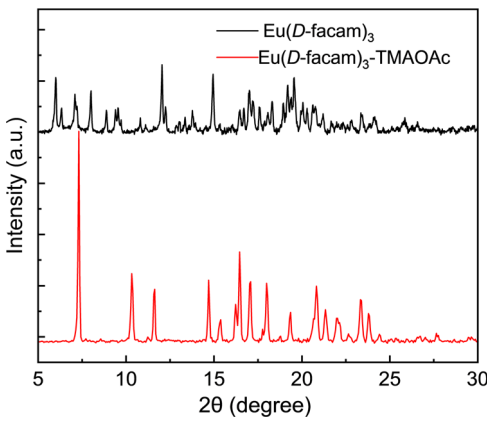

Fig. 8 Powder X-ray diffraction spectra of Eu(D-facam)$_3$ and Eu(D-facam)$_3$-TMAOAc.

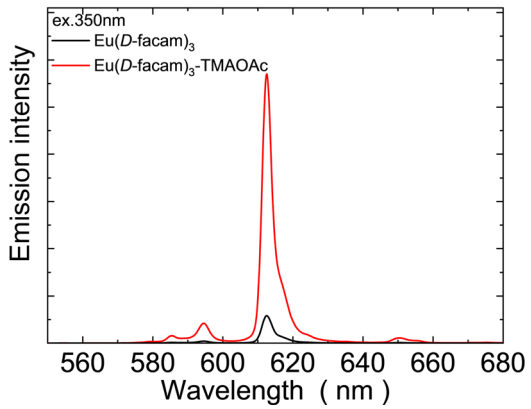

Fig. 9 Emission spectra of Eu(D-facam)$_3$ and Eu(D-facam)$_3$-TMAOAc in acetone. The excitation wavelength was 350 nm.

intensity than that of Eu(D-facam)$_3$. Correspondingly, the measured emission lifetime of Eu(D-facam)$_3$-TMAOAc (363.0 μs) was longer than that of Eu(D-facam)$_3$ (211.3 μs). Therefore, this new Eu(III) hybrid material, Eu(D-facam)$_3$-TMAOAc, exhibited outstanding luminescence performance in both solid and solution states.

Conclusions

This study presented a new Eu(III) hybrid material, (Eu(D-facam)$_3$-TMAOAc), prepared through a simple synthesis method, which is based on the deepening of luminescence improvement in our previous research. Differing from the earlier solution system, this study mainly targeted a solid system which is more suitable for practical applications. Compared to single complexes, Eu(D-facam)$_3$-TMAOAc exhibited significant improvements in the luminescence, circular polarization, and thermal stability. This novel Eu(III) hybrid material well maintained its structure and luminescence properties even after 24 h of heat treatment at 200 °C. The enhancement was primarily attributed to its chain structure, in which TMAOAc acted as a bidentate-bridging molecule, linking with Eu(D-facam)$_3$ at a 1 : 1 ratio. In addition, outstanding luminescence performance of Eu(D-facam)$_3$-TMAOAc was achieved in both solid and solution states. This novel Eu(III) hybrid material has considerable potential for applications, such as in CPL luminophores and bioassays.

Conflicts of interest

There are no conflicts to declare.

Acknowledgements

This work was partly supported by JSPS KAKENHI (grant numbers 17H06377, 20K05641 and 22H02154). Z. Li, one of the authors, received financial support from JST SPRING grant number JPMJFS2107 and an Initiative for Realizing Diversity in the Research Environment (Japan).

Notes and references

1 W. L. Scaff, D. L. Dyer and K. Mori, *J. Bacteriol.*, 1969, **98**, 246–248.
2 H. Tsukube and S. Shinoda, *Chem. Rev.*, 2002, **102**, 2389–2404.
3 J. Yuan and G. Wang, *J. Fluoresc.*, 2005, **15**, 559–568.
4 S. V. Eliseeva and J.-C. G. Bünzli, *Chem. Soc. Rev.*, 2009, **39**, 189–227.
5 Y. Hasegawa and Y. Kitagawa, *J. Photochem. Photobiol., C*, 2022, **51**, 100485.
6 M. A. Martin, A. I. Olives, B. del Castillo and J. C. Menendez, *Curr. Pharm. Anal.*, 2008, **4**, 106–117.
7 M. D. McGehee, T. Bergstedt, C. Zhang, A. P. Saab, M. B. O'Regan, G. C. Bazan, V. I. Srdanov and A. J. Heeger, *Adv. Mater.*, 1999, **11**, 1349–1354.
8 R. C. Evans, P. Douglas and C. J. Winscom, *Coord. Chem. Rev.*, 2006, **250**, 2093–2126.
9 U. Giovanella, M. Pasini, C. Freund, C. Botta, W. Porzio and S. Destri, *J. Phys. Chem. C*, 2009, **113**, 2290–2295.
10 K. Guido, *Hybrid Materials: Synthesis, Characterization, and Applications*, Wiley-VCH Verlag GmbH & Co. KGaA, Germany, 2007.
11 R. Carr, PhD thesis, Durham University, 2014.
12 C. P. Montgomery, B. S. Murray, E. J. New, R. Pal and D. Parker, *Acc. Chem. Res.*, 2009, **42**, 925–937.
13 G. Muller, *Dalton Trans.*, 2009, 9692–9707.
14 S. M. Jeong, Y. Ohtsuka, N. Y. Ha, Y. Takanishi, K. Ishikawa, H. Takezoe, S. Nishimura and G. Suzaki, *Appl. Phys. Lett.*, 2007, **90**, 211106.
15 D.-W. Zhang, M. Li and C.-F. Chen, *Chem. Soc. Rev.*, 2020, **49**, 1331–1343.
16 F. Zinna and L. Di Bari, *Chirality*, 2015, **27**, 1–13.
17 Y. Kondo, S. Suzuki, M. Watanabe, A. Kaneta, P. Albertini and K. Nagamori, *Front. Chem.*, 2020, **8**, 527.
18 B. Yan, *RSC Adv.*, 2012, **2**, 9304–9324.
19 M. Fernandes, S. S. Nobre, M. C. Gonçalves, A. Charas, J. Morgado, R. A. S. Ferreira, L. D. Carlos and V. de Zea Bermudez, *J. Mater. Chem.*, 2009, **19**, 733–742.
20 Y. Hirai, T. Nakanishi, Y. Kitagawa, K. Fushimi, T. Seki, H. Ito and Y. Hasegawa, *Angew. Chem., Int. Ed.*, 2016, **55**, 12059–12062.
21 S. V. Eliseeva, D. N. Pleshkov, K. A. Lyssenko, L. S. Lepnev, J.-C. G. Bünzli and N. P. Kuzmina, *Inorg. Chem.*, 2010, **49**, 9300–9311.
22 H. Zhang, L. Zhou, J. Wei, Z. Li, P. Lin and S. Du, *J. Mater. Chem.*, 2012, **22**, 3457–3461.
23 J.-C. Rybak, M. Hailmann, P. R. Matthes, A. Zurawski, J. Nitsch, A. Steffen, J. G. Heck, C. Feldmann, S. Götzendörfer, J. Meinhardt, G. Sextl, H. Kohlmann, S. J. Sedlmaier, W. Schnick and K. Müller-Buschbaum, *J. Am. Chem. Soc.*, 2013, **135**, 6896–6902.
24 N. N. Golovnev, M. S. Molokeev, S. N. Vereshchagin and V. V. Atuchin, *J. Coord. Chem.*, 2015, **68**, 1865–1877.
25 A. A. Ansari, A. K. Parchur, M. K. Nazeeruddin and M. M. Tavakoli, *Coord. Chem. Rev.*, 2021, **444**, 214040.

26 X. Li, Y. Xie, B. Song, H.-L. Zhang, H. Chen, H. Cai, W. Liu and Y. Tang, *Angew. Chem., Int. Ed.*, 2017, **56**, 2689–2693.
27 M. L. Aulsebrook, B. Graham, M. R. Grace and K. L. Tuck, *Coord. Chem. Rev.*, 2018, **375**, 191–220.
28 Z. Li, H. Minami, K. Nakamura and N. Kobayashi, *ChemPhysChem*, 2021, **22**, 2511–2516.
29 Z. Li, K. Nakamura and N. Kobayashi, *J. Imaging Soc. Jpn.*, 2021, **61**, 194–199.
30 H. Tsumatori, T. Nakashima and T. Kawai, *Org. Lett.*, 2010, **12**, 2362–2365.
31 K. Binnemans, *Coord. Chem. Rev.*, 2015, **295**, 1–45.
32 W. C. Nieuwpoort and G. Blasse, *Solid State Commun.*, 1966, **4**, 227–229.
33 V. V. Atuchin, A. S. Aleksandrovsky, O. D. Chimitova, T. A. Gavrilova, A. S. Krylov, M. S. Molokeev, A. S. Oreshonkov, B. G. Bazarov and J. G. Bazarova, *J. Phys. Chem. C*, 2014, **118**, 15404–15411.
34 V. V. Atuchin, A. K. Subanakov, A. S. Aleksandrovsky, B. G. Bazarov, J. G. Bazarova, T. A. Gavrilova, A. S. Krylov, M. S. Molokeev, A. S. Oreshonkov and S. Y. Stefanovich, *Mater. Des.*, 2018, **40**, 488–494.
35 M. H. V. Werts, R. T. F. Jukes and J. W. Verhoeven, *Phys. Chem. Chem. Phys.*, 2002, **4**, 1542–1548.
36 C. Görller-Walrand, L. Fluyt, A. Ceulemans and W. T. Carnall, *J. Chem. Phys.*, 1991, **95**, 3099–3106.
37 J. P. Riehl and G. Muller, in *Handbook on the Physics and Chemistry of Rare Earths*, ed. K. A. Gschneidner, Jr., J.-C. G. Bünzli and V. K. Pecharsky, Elsevier, Amsterdam, 2004, 220, 289–357.
38 Y. Hasegawa, M. Yamamuro, Y. Wada, N. Kanehisa, Y. Kai and S. Yanagida, *J. Phys. Chem. A*, 2003, **107**, 1697–1702.
39 J. H. S. K. Monteiro, A. de Bettencourt-Dias and F. A. Sigoli, *Inorg. Chem.*, 2017, **56**, 709–712.
40 L. Thompson, J. Legendziewicz, J. Cybinska, L. Pan and W. Brennessel, *J. Alloys Compd.*, 2002, **341**, 312–322.
41 V. L. Garza and N. Purdie, *J. Phys. Chem.*, 1970, **74**, 275–280.
42 K. Miyata, T. Ohba, A. Kobayashi, M. Kato, T. Nakanishi, K. Fushimi and Y. Hasegawa, *ChemPlusChem*, 2012, **77**, 277–280.
43 H. Minami, M. Miyazato, Z. Li, K. Nakamura and N. Kobayashi, *Chem. Commun.*, 2020, **56**, 13532–13535.
44 C. C. R. Sutton, G. da Silva and G. V. Franks, *Chem. – Eur. J.*, 2015, **21**, 6801–6805.
45 K. Nakamoto, *Infrared and Raman Spectra of Inorganic and Coordination Compounds*, John Wiley & Sons, Inc., Hoboken, 1986.
46 G. Calvez, F. Le Natur, C. Daiguebonne, K. Bernot, Y. Suffren and O. Guillou, *Coord. Chem. Rev.*, 2017, **340**, 134–153.

